J|A|C|S
ARTICLES

Published on Web 04/01/2010

^{1}H NMR, Mechanism, and Mononuclear Oxidative Activity of the Antibiotic Metallopeptide Bacitracin: The Role of D-Glu-4, Interaction with Pyrophosphate Moiety, DNA Binding and Cleavage, and Bioactivity

William M. Tay, Jon D. Epperson, Giordano F. Z. da Silva, and Li-June Ming*

Department of Chemistry and MBIG, University of South Florida, Tampa, Florida 33620-5250

Received December 13, 2009; E-mail: ming@shell.cas.usf.edu

Abstract: The peptidyl antibiotic bacitracin (Bc) is one of the most widely used antibiotics which can bind divalent transition metal ions, including Mn(II), Co(II), Ni(II), Cu(II), and Zn(II). The metal binding is essential for its antimicrobial activity. Previous analysis of the hyperfine-shifted ^{1}H NMR signals of Co(II)−Bc A_1 revealed the structure of the metal binding environment and a potential hydrophobic site important for the bioactivity of this antibiotic. Co(II)−Bc in DMSO shows relatively sharper hyperfine-shifted ^{1}H NMR signals compared with the spectrum acquired in an aqueous solution, allowing more thorough analysis of the signals with 1D and 2D NMR methods. Pyrophosphate and derivatives bind to Co(II)−Bc to form kinetically inert ternary complexes. The coordinated D-Glu-4 is found detached from the metal center of metallobacitracin upon trimetaphosphate binding, implying its role in the antibiotic activity of Bc. We further demonstrate in this report the structure−function relationship on desamido-Bc of low antibiotic activity by the use of NMR, wherein D-Glu-4 is suggested to be important for the bioactivity of Bc. The interaction of the phospho-moiety with Bc is also reflected by DNA binding, wherein metal-free Bc does not bind DNA, whereas various metal complexes of Bc do. Cu(II)−Bc was further demonstrated to bind and oxidatively cleave DNA under reduction conditions in the air. It also exhibited a significant oxidative activity toward catechol oxidation, showing enzyme-like saturation kinetics with $k_{cat} = 7.0 \times 10^{-3}$ s^{-1} and $k_{cat}/K_m = 2.1$ M^{-1} s^{-1} aerobically and $k_{cat} = 0.38$ s^{-1} and $k_{cat}/K_m = 14.7$ M^{-1} s^{-1} in the presence of 32 mM of H_2O_2. The binding of pyrophosphate moiety to metallobacitracin, the detachment of D-Glu-4, and the significant oxidative activity of Cu(II)−Bc provide further insights into the bioactivity of this metallopeptide and Cu−oxygen chemistry.

Introduction

Bacitracin (Bc) is a metal-binding cyclic dodecapeptide isolated from cultures of *Bacillus subtilis* and *B. licheniformis*, exhibiting an antibiotic activity primarily against Gram-positive bacteria.[1,2] It is one of the most widely used antibiotics worldwide in animal feed as a preventive drug for livestock[3,4] and in over-the-counter topical "triple antibiotic" Neosporin and Polysporin ointments.[5] Despite extensive use in the past five decades, bacitracin resistance is still scarce which is mainly mediated by the following mechanisms: (a) efflux by ATP-binding cassette (ABC) transporters as in the *Bacilus* species themselves, *Streptococcus pneumoniae*,[6] and *Enterococcus faecalis*,[7] (b) overproduction of undecaprenol kinase as in *Escherichia coli*,[8,9] and (c) an unknown mechanism related to rhamnose-glucose polysaccharide (RGP) synthesis as in *S. mutans*.[10] Nevertheless, its use in animal feed has been banned in the European Union since 1997 due to the worry of microbial resistance and cross resistance. However, later studies revealed decline in the health of livestock and increase in usage of therapeutic antibiotics in animals as a result of the ban,[11] suggesting proper management of Bc usage in farms is important.

This antibiotic is produced through a nonchromosomal pathway by a peptide synthase as a mixture of many closely related peptides, in which Bc A_1 is the major component with the most potent antibiotic activity.[12,13] Bc A_1 contains a thiazoline ring formed by the condensation of the Ile-1 carboxylate with both the $-NH_2$ and the $-SH$ groups of Cys-2,[12,13] four D-amino acids, and a unique cyclic heptapeptide structure formed via an amide linkage between the side chain of Lys-6 and the C-terminus of Asn-12 (Figure 1). These unusual structural features may protect this peptide from degradation by proteases[14] and offer challenge to total synthesis of this

(1) Ming, L.-J.; Epperson, J. D. *J. Inorg. Biochem.* **2002**, *91*, 46–58.
(2) Brewer, G. A.; Florey, K. *Anal. Profiles Drug Subst.* **1980**, *9*, 1–69.
(3) Hanson, D. J. *Chem. Eng. News* **1985**, *63*, 7–11.
(4) Yagasaki, T. *Food Hyg. Soc. Jpn.* **1986**, *27*, 451–465.
(5) Arky, R. *Physicians' Desk Reference for Nonprescription Drugs*, 18th ed.; Medical Economics Company: Montvale, NJ, 1997.
(6) Becker, P.; Hakenbeck, R.; Henrich, B. *Antimicrob. Agents Chemother.* **2002**, *46*, 2034–2041.
(7) Manson, J. M.; Keis, S.; Smith, J. M. B.; Cook, G. M. *Antimicrob. Agents Chemother.* **2004**, *48*, 3743–3748.
(8) Cain, B. D.; Norton, P. J.; Eubanks, W.; Nick, H. S.; Allen, C. M. *J. Bacteriol.* **1993**, *175*, 3784–3789.
(9) El Ghachi, M.; Bouhss, A.; Blanot, D.; Mengin-Lecreulx, D. *J. Biol. Chem.* **2004**, *279*, 30106–3011.
(10) Tsuda, H.; Yamashita, Y.; Shibata, Y.; Nakano, Y.; Kogai, T. *Antimicrob. Agents Chemother.* **2002**, *46*, 3756–3764.
(11) Casewell, M.; Friis, C.; Marco, E.; McMullin, P.; Phillips, I. *J. Antimicrob. Chemother.* **2003**, *52*, 159–161.
(12) Siegel, M. M.; Huang, J.; Lin, B.; Tsao, R. *Biol. Mass Spectrom.* **1994**, *23*, 196–204.

10.1021/ja910504t

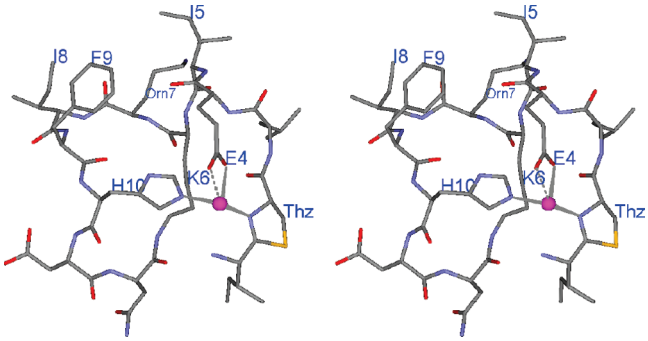

Figure 1. Stereo view of bacitracin A_1 according to NMR and molecular dynamic calculations.[13] The metal binding ligands have been determined to be the thiazoline (Thz) nitrogen, the side chains of His-10 and D-Glu-4, and presumably an open site or sites for water binding.

drug.[15,16] Bc requires a divalent metal ion for its antimicrobial activity[17,18] and can form complexes with several divalent metal ions, including Mn(II), Co(II), Ni(II), Cu(II), and Zn(II),[19,20] as determined by the use EPR,[21] electrophoresis,[22] and microcalorimetric[23] methods. The latter[23] revealed that the metal-binding affinity constants (M^{-1}) followed Cu(II) (6460) > Ni(II) (1381) > Co(II) (214.0) > Zn(II) (74.36) > Mn(II) (weak), whereas the antibiotic activity is not affected by the affinity constant. We reported a detailed analysis of the hyperfine-shifted ^{1}H NMR features of the Co(II) complexes of a few Bc congeners in aqueous solution by means of 1D and 2D NMR techniques.[24] The NMR studies unambiguously revealed the metal coordination sphere, with the metal binding ligands being the thiazoline ring nitrogen, the Nε nitrogen of His-10, and the carboxylate side chain of D-Glu-4. A correlation between the structure and the activity of this antibiotic metallopeptide has also been suggested.

Metal(II)−Bc complexes bind tightly to C_{55}-isoprenyl pyrophosphate,[25] which prevents the lipid dolichol pyrophosphate from being hydrolyzed by a membrane pyrophosphatase and subsequently inhibiting N-glycosylation of nascent proteins in the lumen of the endoplasmic reticulum. This inhibition serves as the key step in the inhibition of cell wall synthesis by this antibiotic.[26] Although a pyrophosphate-metal-Bc ternary complex was proposed,[27] detailed binding and structural information about this ternary complex has not yet been presented. The binding mode of D-Glu-4 side chain in Bc seems to reflect the activity of this antibiotic;[24] however, whether or not it is involved in the interaction with lipid pyrophosphate and its role in this interaction, if any, was not concluded. Atomic force microscopy revealed that the surface of *S. aureus* is affected by Zn(II)-complex, but not by Bc alone.[23] We report herein the study of (a) Co(II)−Bc and the inactive Co(II)−(desmido-Bc) to further establish their structure−activity correlation, (b) the binding of several pyrophosphate-containing compounds to Co(II)−Bc complex, (c) the binding of plasmid to various metallobacitracins, (d) aerobic oxidative cleavage of DNA by Cu(II)−Bc in the presence of ascorbic acid, and (e) oxidation of catechol by Cu(II)−Bc in the presence and absence of H_2O_2 in the air. The pyrophosphate-containing compounds form kinetically inert ternary complexes with Co(II)−Bc via the binding of the pyrophosphate moiety to the Co(II) cdenter, with a possible change of the coordination mode of D-Glu-4. The results have provided further insight into the mechanism of metallobacitracins as well as Cu-centered oxidation chemistry.

Experimental Section

Chemicals and Sample Preparations. The crude Bc mixture was purchased from Sigma-Aldrich (St. Louis, MO), from which several congeners can be isolated by means of reverse phase HPLC.[24] The Co(II) complexes of Bc were prepared by direct addition of $Co(NO_3)_2$ solution into Bc solutions. The ternary complexes of Co(II)−Bc with pyrophosphate derivatives were prepared at 2−4 mM by direct mixing equal molar amounts of the components together at pH 5.0, followed by removal of the precipitate. The presence of 3 M guanidinium chloride to farnesyl pyrophosphate−Co(II)−Bc sample reduced the amount of precipitation. The ^{1}H NMR spectrum of this complex was acquired immediately after adjusting the pH to 5.0 to minimize hydrolysis of the pyrophosphate.[28] The presence of buffer significantly decreases the solubility of Co(II)−Bc for NMR studies, thus is avoided. All other reagents were obtained from commercial sources; $CuSO_4$ from Fisher Scientific Co. (Fair Lawn, NJ), pyrocatechol (~99%) and pyrophosphate and derivatives from Sigma-Aldrich, and 3-methyl-2-benzothiazolinone hydrazone (MBTH) hydrochloride monohydrate (98%) from Acros (NJ).

The derivative desamido-Bc was prepared by dissolving 100 mg of the Bc mixture in 4 mL of 0.1 N sodium hydroxide, shaked at 37 °C for 2 h, then neutralized with 1.0 N HCl to pH 5.0. The solution was then lyophilized and dissolved in 600 μL of water and isolated with the reverse-phase Zorbax column (Rx-C8, 9.4 mm × 24 cm; Agilent Technologies, Santa Clara, CA).

NMR Experiments. ^{1}H NMR spectra were acquired on a Bruker AMX360 operating at 360.13 MHz or a Bruker DRX250 spectrometer at 250.13 MHz. A 90° pulse with presaturation for solvent suppression was used for the acquisition of 1D ^{1}H NMR spectra of 8K data points. The "super WEFT" technique[29] (D_1−180°−τ−90°) was employed for data acquisition of samples in H_2O to suppress the solvent and diamagnetic signals by minimizing the delays D_1 and τ. The ^{1}H NMR chemical shift was referenced to the internal HDO signal assigned to 4.8 ppm. A line-broadening factor of 10−30 Hz was introduced to the spectra via exponential multiplication prior to Fourier transformation to enhance the signal-to-noise ratio.

The 1D saturation transfer difference spectrum was obtained with the FIDs added and subtracted upon the application of a decoupler pulse set on a signal of interest and at a reference position, respectively, for 30−80 ms followed by a 0.3−10 Hz exponential

(13) Morris, M. *Biol. Mass Spectrom.* **1994**, *23*, 61–70.
(14) Pfeffer, S.; Hohne, W.; Branner, S.; Wilson, K.; Betzel, C. *FEBS Lett.* **1991**, *285*, 115–119.
(15) Lee, J.; Griffin, J. H. *J. Org. Chem.* **1996**, *61*, 3983–3986.
(16) Wagner, B.; Schumann, D.; Linne, U.; Koert, U.; Marahiel, M. A. *J. Am. Chem. Soc.* **2006**, *128*, 10513–10520.
(17) Storm, D. R.; Strominger, J. L. *J. Biol. Chem.* **1974**, *249*, 1823–1827.
(18) Piacham, T.; Isarankura-Na-Ayudhya, C.; Nantasenamat, C.; Yainoy, S.; Ye, L.; Bulow, L.; Prachayasittikul, V. *Biochem. Biophys. Res. Commun.* **2006**, *34*, 925–930.
(19) Garbutt, J. T.; Morehouse, A. L.; Hanson, A. M. *J. Agric. Food Chem.* **1961**, *9*, 285–289.
(20) Scogin, D. A.; Mosberg, H. I.; Storm, D. R.; Gennis, R. B. *Biochemistry* **1980**, *19*, 3348–3352.
(21) Seebauer, E. G.; Duliba, E. P.; Scogin, D. A.; Gennis, R. B.; Belford, R. L. *J. Am. Chem. Soc.* **1983**, *105*, 4926–4929.
(22) Castagnola, M.; Rossetti, D. V.; Inzitari, R.; Lupi, A.; Zuppi, C.; Cabras, T.; Fadda, M. B.; Onnis, G.; Petruzzelli, R.; Giardina, B.; Messana, I. *Electrophoresis* **2004**, *25*, 846–852.
(23) Qi, Z. D.; Lin, Y.; Zhou, B.; Ren, X.-D.; Pang, D.-W.; Liu, Y. *J. Membr. Biol.* **2008**, *225*, 27–37.
(24) Epperson, J. D.; Ming, L.-J. *Biochemistry* **2000**, *39*, 4037–4045.
(25) Storm, D. R.; Strominger, J. L. *J. Biol. Chem.* **1973**, *248*, 3940–3945.
(26) Higashi, Y.; Strominger, J. L.; Sweeley, C. C. *J. Biol. Chem.* **1970**, *245*, 3697–3702.
(27) Stone, K. J.; Strominger, J. L. *Proc. Nat. Acad. Sci. U.S.A.* **1971**, *68*, 3223–3227.
(28) Goodman, DeW. S.; Popjak, G. *J. Lipid Res.* **1960**, *1*, 286–300.
(29) Inubushi, T.; Becker, E. D. *J. Magn. Reson.* **1983**, *51*, 128–133.

multiplication prior to the Fourier transformation. Owing to the fast relaxation rates of the hyperfine-shifted signals, saturation transfer was investigated by irradiating the hyperfine-shifted signals and observing possible saturation transfer to the diamagnetic signals, and by the use of the EXSY pulse sequence with a short mixing time of a few ms. The NOESY spectra were obtained with the standard pulse sequence and 10−30 ms mixing time and the TOCSY spectra were obtained using the MLEV-17 spin-lock of 8−30 ms. The 2D spectra were acquired with 1K × 128 data points, zero-filled to 1K × 1K, processed with a sine-bell-squared window, and followed by baseline correction.

DNA Interaction and Cleavage. Oxidative DNA cleavage by Cu(II)−Bc was studied under reduction conditions in the presence of excess amount of ascorbic acid following the previously protocol with a slight modification.[30] Typically, the plasmid DNA (150−200 ng) was incubated with 75.0 μM Cu(II)−Bc and 5.0 mM ascorbic acid in 100.0 mM HEPES at pH 7.0 and 25 °C over a time course (0−60 min), then analyzed in a 1.0% agarose gel stained with ethydium bromide and photographed on a transilluminator.

Oxidative Activity. The catechol oxidation assay was carried out as previously described.[30] Different concentrations of the substrate catechol (CA) with equivalent concentration of MBTH were incubated with Cu(II)−Bc in 100 mM HEPES buffer at pH 7.0 in the presence and absence of different amounts of H_2O_2. The oxidized *o*-quinone binds to MBTH to form a red adduct, which was monitored at 500 nm (ε = 32, 500 $M^{-1}cm^{-1}$)[31] on a Varian Cary50 spectrophotometer and the initial rate measured. The kinetic constants K_m and k_{cat} were determined by nonlinear fitting of the data to an appropriate rate law. For anaerobic experiments, the dissolved oxygen from all components was removed by multiple freeze-and-thaw cycles on a vacuum-argon line, and the solutions were transferred with a gastight syringe and the rates measured as above.

The substrate 4,5-dichlorocatechol (DCC) with a much slower turnover rate was used to show the interaction between Cu(II)−Bc and a catechol substrate. DCC was dissolved in DMF and gradually titrated into a buffer solution of Cu(II)−Bc (300.0 μM). The spectra were obtained on the Varian Cary50 spectrophotometer with the solvent as the baseline. The molar absorptivity of the [Cu(II)−Bc]−DCC complex at 304 nm was plotted with respect to the DCC concentration, and the data were fitted with nonlinear regression to determine the affinity constant, K_{DCC}.

The Job plot is a continuous variation technique which allows the determination of the stoichiometry of metal−ligand complexes.[32,33] The stoichiometry for Cu(II)−Bc binding with a ligand such as CA or DCC to form a ternary complex of $[Cu(II)-Bc]_x-CA/DCC)_y$ was determined with Job plot, wherein the concentrations of Cu(II)−Bc and the ligand (DCC or CA) were varied while keeping the total concentration constant (e.g., [Cu(II)−Bc] + [CA] = 50.0 μM). The output as absorption (at 304 nm for the binding of the inert substrate DCC) or activity (for the binding of CA to form the reactive intermediate complex [Cu(II)−Bc]−CA during CA oxidation) is plotted as a function of the mole fraction of the catalyst (X_{Cu-Bc}) or the ligand/substrate (X_{DCC} or X_{CA}). The ratio of X_{Cu-Bc}: $X_{DCC/CA}$ at which the absorbance or activity reaches the maximum in the plot reflects the stoichiometry of the [Cu(II)−Bc]−DCC/CA complex under the experimental conditions.

Results and Discussion

Co(II)−Bc in Hydrophobic Environment. High-spin Co(II) has been utilized as a probe for the characterization of the metal-binding site(s) of metallo-biomolecules and their interactions with ligands via the assignment of the isotropically shifted ^{1}H NMR signals.[34−36] The Co(II)−Bc complex in aqueous solution exhibits about 20 well resolved isotropically shifted ^{1}H NMR signals which have been unambiguously assigned by means of 1D and 2D NMR techniques.[24] For example, the α-, β-, γ-, and NH-protons of D-Glu-4 are found at −6.4, −3.2, −14.8/34, and −60.8 ppm, respectively (Figure 2D). D-Glu-4 may play an important role in Bc action since it is not coordinated to the metal ion in those Bc congeners and derivatives of low potency, including Bc A_2 and F.[24]

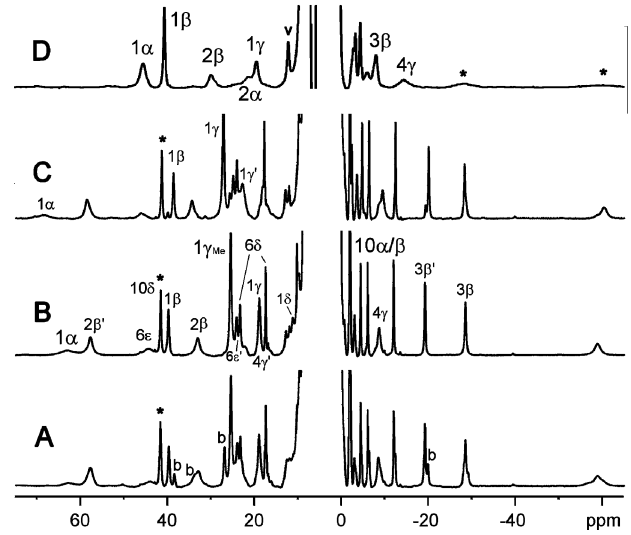

Figure 2. The hyperfine-shifted ^{1}H NMR spectra of the Co(II) complex of crude Bc (A), Co(II)−Bc A_1 (B), and Co(II)−Bc B_1 (C) in DMSO. Spectrum (D) is the Co(II) complex of crude Bc in water at pH 5.0. The solvent exchangeable signals are labeled with asterisks and the signals due to Co(II)−Bc B_1 in (A) is labeled with b's. The signal v in (D) is due to the γ protons of Val-1 in Co(II)−Bc B_1.

A proposed antibacterial action of metallobacitracin is that it binds with sugar-carrier lipid-pyrophosphate which prevents the delivery of the sugar for bacterial cell well synthesis.[26] Such action would put metallobacitracin in a less hydrophilic environment. Thus, the NMR spectrum of Co(II)−Bc in DMSO was acquired to mimic metallobacitracin in such environment. The hyperfine-shifted ^{1}H NMR spectrum of the Co(II) complexes of crude Bc in DMSO is shown in Figure 2A along with the spectra of Co(II)−Bc A_1 (Figure 2B) and Co(II)−Bc B_1 (Figure 2C), significantly different from that in aqueous media (Figure 2D). The most notable difference is the clear detection of the His-10 signals of the complex in DMSO (discussed later). A few downfield hyperfine shifted signals can be readily assigned to Ile-1 or Val-1 which is the only difference between Bc A_1 and B_1. The signals at 39.9, 25.5, 19.0, and 11.2 ppm observed only in Co(II)−Bc A_1 (Figure 2B) can be assigned to Ile-1, whereas the signals at 38.7, 27.6, and 22.5 ppm in Co(II)−Bc B_1 (Figure 2C) can be assigned to Val-1.

The Co(II)-bound Bc does not undergo chemical exchange with free Bc in DMSO, which prevents signal assignment by the use of exchange-based saturation transfer techniques applied to the study in aqueous solutions.[24] Titration of D_2O into

(30) da Silva, G. F. Z.; Tay, W. M.; Ming, L.-J. *J. Biol. Chem.* **2005**, *280*, 16601–16609.
(31) Srivatsan, S. G.; Nigam, P.; Rao, M. S.; Verma, S. *Appl. Catal., A* **2001**, *209*, 327–334.
(32) Huang, C. Y. *Methods Enzymol.* **1982**, *87*, 509–525.
(33) Wei, X.; Ming, L.-J. *Inorg. Chem.* **1998**, *37*, 2255–2262.
(34) Bertini, I.; Luchinat, C. *NMR of Paramagnetic Molecules in Biological Systems*; Benjamin/Cummings: Menlo Park, CA, 1986.
(35) Ming, L.-J. In *Physical Methods in Bioinorganic Chemistry, Spectroscopy and Magnetism*; Que, L., Jr., Ed.; University Science Books: Sausalito, CA, 2000.
(36) Bertini, I.; Luchinat, C. *Adv. Inorg. Biochem.* **1984**, *6*, 71–111.

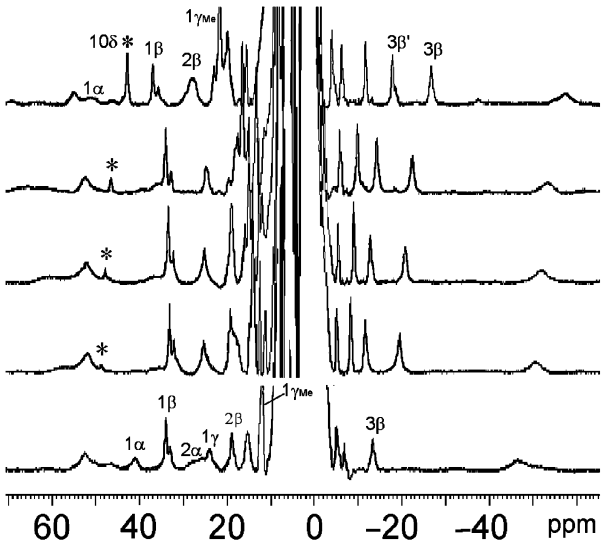

Figure 3. Addition of D_2O (0, 20, 40, 60, and 200 μL from top) to 400 μL of Co(II)−Bc in d_6-DMSO. The signals which can be clearly recognized are labeled. The solvent exchangeable imidazolyl NH signal of the coordinated His is marked with an asterisk.

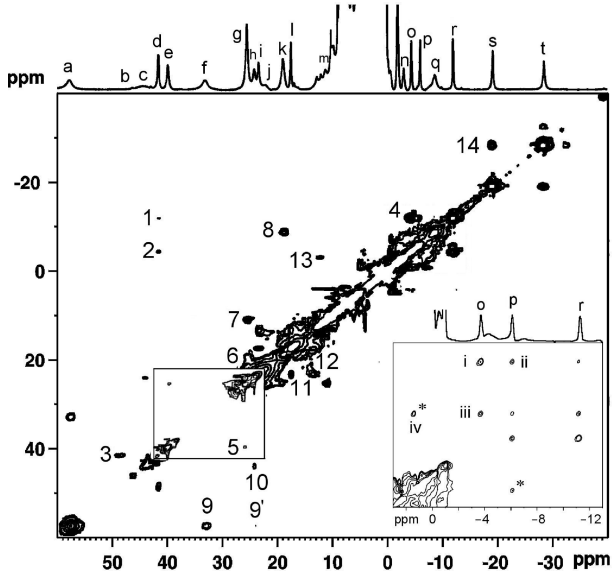

Figure 4. NOESY spectrum of Co(II)−Bc with a mixing time of 30 ms. The insets show through-bond interactions of $1\beta-1\gamma$ and in His-10 (i−iv) from TOCSY spectrum (mixing time 30 ms).

Co(II)−Bc in DMSO results in gradual shift of the signals, which allows correlation of a few signals of the complex in DMSO with those in aqueous solutions to be established (labeled in Figure 3). For example, the His-10 solvent exchangeable $N_\delta H$ signal (Figure 3, asterisked) at 41.6 ppm shifts downfield (47 ppm) upon the addition of a small amount of D_2O and eventually disappears when 60 μL of D_2O is added.

The small size and the paramagnetism of paramagnetic metal complexes can diminish cross relaxation and coherance transfer.[34,35] Nevertheless, clear 2D NMR spectra of Co(II)−Bc A_1 were successfully obtained (Figure 4) which was not obtainable in aqueous solutions.[24] The His-10 ring NH signal displays cross peaks in the NOESY spectrum to the two β protons (peaks 1 and 2, Figure 4) at −11.9 (T_1 = 76 ms) and −4.3 ppm (102 ms) and to the $C_\delta H$ proton at 48 ppm (peak 3). The His-10 β protons display cross peaks in the TOCSY

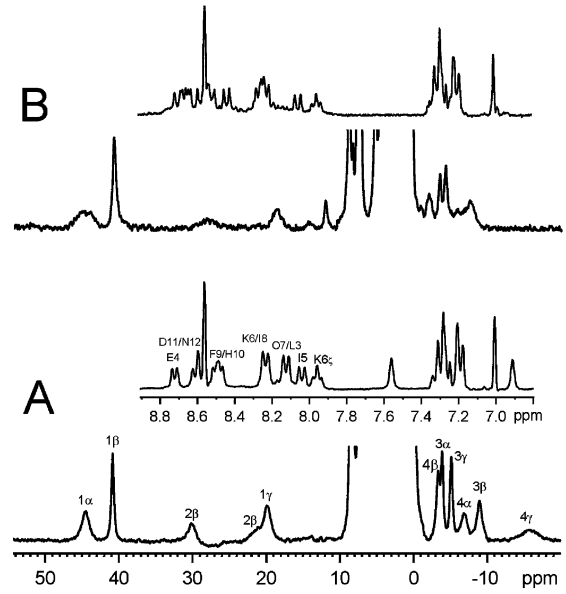

Figure 5. ^{1}H NMR spectrum of Co(II)−Bc A_1 (A) and Co(II)−desamido-Bc (B). The insets are the corresponding apo forms of the antibiotic which show the disappearance of the two amide NH_2 signals of Asn-12 at 6.91 and 7.58 ppm upon hydrolysis.

spectrum to each other and to the α proton at −6 ppm (120 ms) (inset, Figure 4) and the spin system NH−C_αH−$C_\beta H_2$ of His-10 is established, wherein the signals o and r are the $C_\beta H_2$ pair, p the C_αH proton, and iv reveals the solvent exchangeable peptidyl NH (asterisked). These assignments confirm the binding of His-10 to Co(II) via the N_ε atom, which may render the N_δH proton to be close to the β-CH_2 protons to produce the NOESY cross peaks (**1** and **2** in Figure 4), whereas the N_εH proton of N_δ-coordinated His cannot be near the β-CH_2 protons under any configuration. Furthermore, the C_εH and C_δH signals of N_ε-coordinated His side chains are typically broadened beyond detection in Co(II) complexes and metalloproteins[34,35] which is consistent with the data presented here.

Several intense signals in the NOESY spectrum (Figure 4) can also be readily assigned to geminal pairs, including **4**, **8**, **9**, **10**, and **14**. On the basis of the structure of the complex in aqueous solution,[24] Cys-2-β (thiazoline), Lys-6-ε,δ, His10-β, Glu-4-β, and Ile-3-β proton pairs are within 5.5 Å from the metal which are thus expected to afford these cross peaks. Of these, the Ile-3 signals s and t are identified in the D_2O titration; signals c and h (with cross peak **10**) are from Lys-6-ε with one proton closer to the metal to exhibit the broad signal c; and peak 4 is due to His10-β (discussed above). Peak **8** is possibly due to Glu-4-γ protons which were determined to shift to the opposite directions in Co(II)−Bc in aqueous solution;[24] and peak **9** is most likely to be attributed to the β pair of the coordinated thiazoline (Cys-2) ring near the metal. The detection of cross peak **9′** indicates the proximity of one Cys-2-β proton (a) and one Lys-6-ε proton (h).

^{1}H NMR of Co(II)−Desamido-Bc A_1. In order to gain further insight into the structure−activity relationship of Bc, desamido-Bc A_1 of a low potency was prepared by hydrolyzing Asn-12 of Bc A_1 to an Asp ([M + H^+], *m/z* 1423.4). As a result of the hydrolysis, the two resolved solvent exchangeable ^{1}H NMR signals of Asn-12 amide NH_2 at 7.58 and 6.91 ppm in Bc A_1 (inset, Figure 5A) disappear in the desamido derivative (inset, Figure 5B), along with noticeable shifts for the peptidyl NH protons of Leu-3, Orn-7, Asp-11, and Asn-12. The significant

changes in the coordination chemistry of Bc F (which only binds through His10) and Bc A_2 were suspected to contribute to the lack of their antibiotic activities.[24] The Ile-1 α-, β-, and γ-CH_2 protons (45.1, 40.2, and 19 ppm, respectively) and the Leu-3 α-, β-, and γ-protons (−3.0, −7.0, and a −3.8 ppm, respectively) in the Co(II) complex of desamido-Bc A_1 are only slightly different from those of Bc A_1, indicating that they have configuration similar to those in Co(II)−Bc A_1.

The signals at 11.0 and −2.0 ppm in the Co(II)−desamido-Bc A_1 do not seem to match with counterparts in Co(II)−Bc A_1. The 11 ppm signal shows saturation transfer in a 1D NOE difference experiment to a diamagnetic signal at 1.1 ppm, while the upfield shifted signal at −2.0 ppm correlates to a signal at 0.8 ppm, consistent with the methylene protons of Ile5 that are in close proximity of the Co(II) ion. The hyperfine shifted signals due to the Glu-4 α, β, and γ protons in Co(II)−desamido-Bc A_1 are not detected, suggesting that Glu-4 is not bound to the metal. Likewise, Glu-4 in those Bc congeners of low antibiotic potency, including Bc A_2 and F, does not coordinate to the metal on the basis of missing hyperfine-shifted ^{1}H NMR signals.[24] This is in contrast to other biologically active congeners, such as Bc A_1, B_1, and B_2 with nearly identical hyperfine-shifted ^{1}H NMR features.[24] Therefore, the active Bc congeners may require a coordinated Glu-4 to exhibit activity upon binding with the sugar-carrying lipid pyrophosphate. In order to gain further information about the action of Bc and to reveal the role of Glu-4 in Bc function, the binding of pyrophosphate and derivatives to Co(II)−Bc was investigated.

Pyrophosphate and Phosphate Binding. The binding of metallobacitracin complex with bactoprenyl pyrophosphate is considered the key step in the inhibition of bacterial cell wall synthesis.[25−27] Small pyrophosphate-containing molecules are utilized as model systems for the investigation of the binding of lipid pyrophosphate with metallobacitracin. Addition of several pyrophosphate derivatives to Co(II)−Bc results in significant precipitation, presumably due to a pyrophosphate−metallobacitracin complex since neither solution alone precipitates. The precipitation can presumably remove lipid pyrophosphate effectively which inhibits cell wall synthesis. The supernatant upon addition of sodium pyrophosphate to Co(II)−Bc shows several new isotropically shifted ^{1}H NMR signals (Figure 6A) which are significantly different from the signals of Co(II)−Bc (Figure 2), indicating binding of pyrophosphate to the metal center. These new signals do not reveal any noticeable saturation transfer to signals in the diamagnetic region that are attributed to unbound pyrophosphate or Bc. Thus, the ternary complex must be kinetically inert which is also expected to be the case in vivo (despite the higher concentrations in the NMR experiments than those in vivo) since kinetic inertness is independent of concentration. The pyrophosphate in this ternary complex does not show detectable ^{31}P NMR signals, indicating its binding to the paramagnetic Co(II) center which results in the broadening of the signals beyond detection.

A TOCSY experiment on the upfield region of this sample reveals a spin pattern that is consistent with Leu-3 (Figure 7). In which, cross peak **1** is due to a weak interaction between the two δ-CH_3 groups; **2** and **3**, δ-CH_3/γ-CH interactions; **4** and **6**, γ-CH/β-CH_2 and γ-CH/α-CH interactions; and **5**, β-CH_2/α-CH interaction. The detection of Leu-3 in the upfield region as in the parent Co(II)−Bc A_1 complex[24] indicates that the environment of Leu-3 may not be significantly affected by pyrophosphate binding. The three-spin system CH_2−CH may be assign-

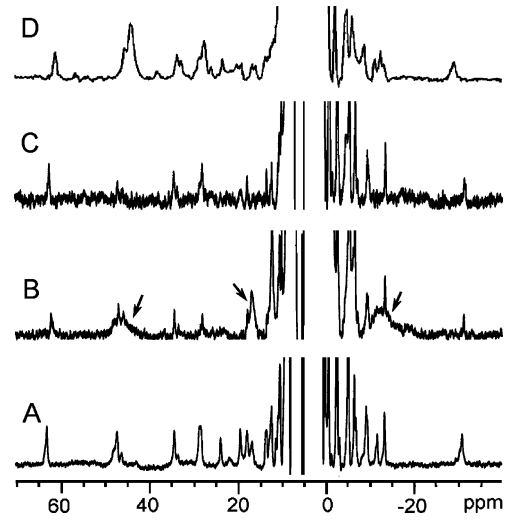

Figure 6. ^{1}H spectra (250.13 MHz and 298 K; samples in D_2O at pH meter reading of pH* 5.4) of Co(II)−Bc upon binding of (A) pyrophosphate, (B) trimetaphosphate, (C) triphosphate, and (D) farnesyl pyrophosphate in the presence of 3 M guanidinium chloride. The sharp features in (B) are due to hydrolysis of trimetaphosphate into triphosphate (cf. C), while the broad features are due to labile trimetaphosphate complex (marked).

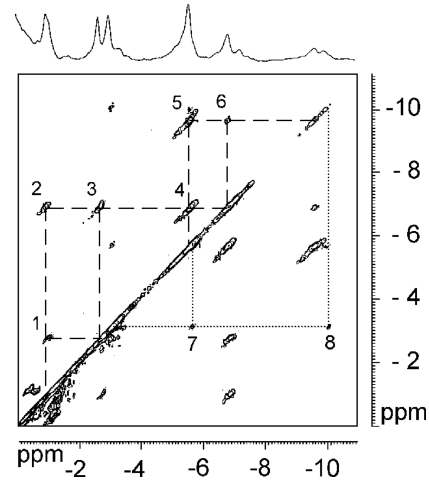

Figure 7. TOCSY spectrum (250.13 MHz, 298 K, mixing time 30 ms) of the upfield region of pyrophosphate−Co(II)−Bc ternary complex in D_2O pH* 5.5 (pH meter reading) reveals a spin pattern that is consistent with Leu3 (cross peaks 1−6). A CH_2CH spin system is also revealed (7, 8).

able to the coordinated His10, analogous to the signals observed in the parent complex (inset, Figure 4).

Phosphate in the low millimolar range does not perturb the spectral features of Co(II)−Bc, indicating very weak interactions. A pyrophosphate moiety is thus essential for tight binding to metal−Bc complexes. Moreover, both pyrophosphoesters and phosphoesters with long hydrophobic chains were reported to bind to metallobacitracin tightly,[25] indicating that hydrophobic interaction is also important for the formation of complexes with metallobacitracin.

Triphosphate and Trimetaphosphate Binding. The triphosphate complex of Co(II)−Bc shows sharp isotropically shifted signals with no detectable saturation transfer to other signals (Figure 6C), indicating the formation of a kinetically inert complex as in the case of the pyrophosphate ternary complex discussed above. The overall spectral features of this complex are very similar to those of the pyrophosphate−(Co−Bc) ternary complex, indicating similar metal binding environments of these

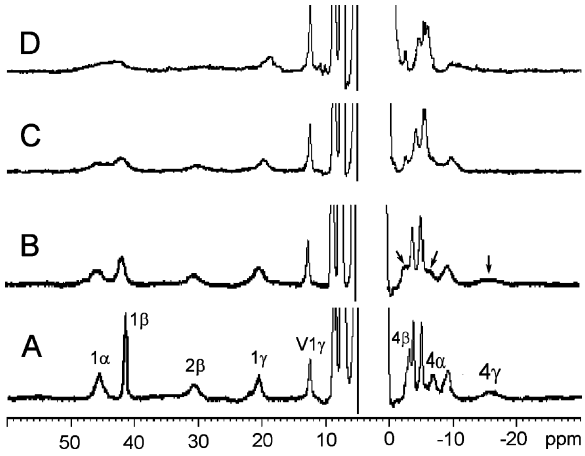

Figure 8. Addition of 0 (A), 0.25 (B), 0.5 (C), and 1.0 equiv of trimetaphosphate to Co(II)−Bc (250.13 MHz and 298 K; sample in D_2O at pH* 5.4). The marked signals are due to Glu4 protons.

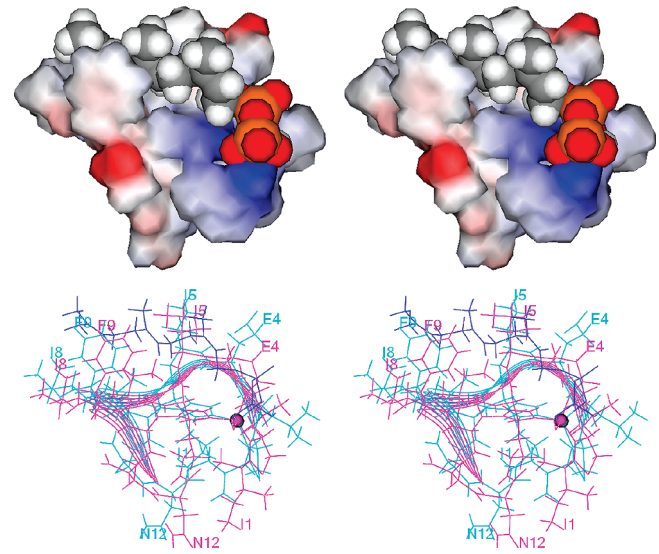

Figure 9. Farnesyl pyrophosphate-bound metallobacitracin determined by the use of molecular mechanics calculations (MM3, BioMedCAChe 6.0; Fujitsu, Beaverton, OR). The pyrophosphate moiety is bound to the metal center with the hydrophobic farnesyl moiety sitting in the hydrophobic pocket formed by Ile5, Ile8, and D-Phe9. The D-configuration of Phe9 is essential for such interaction. The bottom structure shows a significant change at the hydrophobic pocket upon farnesyl pyrophosphate binding (before, pink; after, cyan). E4 is presumably detached upon farnesyl pyrophosphate binding and the amino group is H-bonded to the pyrophosphate moiety to balance the charge.

two complexes with the pyrophosphate moiety bound to the metal center.

The trimetaphosphate ternary complex, however, gives both sharp and broad isotropically shifted signals a few hours after its preparation (Figure 6D). The sharp signals are due to the triphosphate complex (Figure 6C) after hydrolysis of the trimetaphosphate and are not detected in freshly prepared samples (see later). Saturation transfer was observed between the broad hyperfine shifted signals in this ternary complex and some diamagnetic signals, indicating that the trimetaphosphate−(Co−Bc) ternary complex is kinetically labile and the broadening of the signals is due to the presence of chemical exchange,[34,35] allowing the use of saturation transfer or titration method to assign some key signals for the interaction with pyrophosphate moiety.

The hyperfine-shifted ^{1}H NMR signals of Co(II)−Bc are affected to different extents by the addition of trimetaphosphate. Herein, the signals corresponding to the D-Glu-4 α-, *β*-, and *γ*-protons of Co(II)−Bc are greatly influenced and disappear upon formation of the ternary complex (marked signals in Figure 8), indicating that the D-Glu-4 carboxylate side chain undergoes fast exchange and is possibly detached from the Co(II) ion upon trimetaphosphate binding.

The binding of D-Glu-4 side chain to the metal is essential for the antibiotic activity of Bc since it is not bound to the metal in the inactive Bc A_2 and F congeners[24] and desamido-Bc derivative discussed above. Its binding may afford an appropriate structure such as the formation of a hydrophobic site composed of Ile-5, Ile-8, and D-Phe-9.[24] The result shown here corroborates that D-Glu-4 plays an important role for the binding of pyrophosphate moiety to metallobacitracin. The detachment of D-Glu-4 upon the binding of negatively charged pyrophosphate may be important to partially balance the charge at the metal center and/or to reduce steric crowding around the metal. Detachment of an endogenous ligand upon binding of an external ligand or the substrate was previously observed or proposed in several metalloenzyme systems which has been suggested to be catalytically important in these enzymes, including the coordinated Glu in quercetin 2,3-dioxygenase,[37] His in Cu,Zn-superoxide dismutase,[38,39] and Tyr in Fe-dioxygenase,[40] serralysin,[41] and astacin.[42] The several signals due to Leu-1 are also significantly affected by trimetaphosphate binding, suggesting that the N-terminal amino group may be interacting with the coordinated pyrophosphate moiety (see below).

Farnesyl Pyrophosphate Complex. Farnesyl pyrophosphate contains a C_{15}-isoprenoid chain which can serve as a biochemical model for the investigation of the interaction of metallobacitracin with lipid pyrophosphate. The addition of farnesyl pyrophosphate to Co(II)−Bc at pH 5.5 in the presence of 3 M guanidinium chloride affords a resonably soluble complex with a ^{1}H NMR spectrum similar to the spectrum of pyrophosphate−(Co−Bc) complex (Figure 6). This result indicates that farnesyl pyrophosphate binds to the metal center of Co(II)−Bc via its pyrophosphate moiety while its hydrocarbon chain is bound to the hydrophobic pocket of the drug, which can be expected also to be the case for the binding of lipid pyrophosphate to metallobacitracin in vivo.

A significant decrease in energy by ∼200 kJ/mol was obtained from MM3 molecular mechanics calculation for the binding of farnesyl pyrophosphate to metallobacitracin, wherein the farnesyl chain fits into the hydrophobic site composed of Ile-5, Ile-8, and D-Phe-9 (Figure 9). When metallobacitracin is superimposed onto its farnesyl pyrophosphate-bound complex with the metal, the coordinated His and thiazoline, Ile-8, and Orn-7 as the matching points, an rms of 0.36 Å was obtained. The largest configurational changes are seen at (a) the N-terminal amino group which becomes H-bonded with the bound pyrophosphate moiety, (b) D-Glu-4 which is detached from the metal

(37) Steiner, R. A.; Kooter, I. M.; Dijkstra, B. W. *Biochemistry* **2002**, *41*, 7955–7962.
(38) Banci, L.; Bencini, A.; Bertini, I.; Luchinat, C.; Piccioli, M. *Inorg. Chem.* **1990**, *29*, 4867–4873.
(39) Bertini, I.; Luchinat, C.; Ming, L.-J.; Piccioli, M.; Sola, M.; Valentine, J. S. *Inorg. Chem.* **1992**, *31*, 4433–4435.
(40) Orville, A. M.; Lipscomb, J. D.; Ohlendorf, D. H. *Biochemistry* **1997**, *36*, 10052–10066.
(41) Park, H. I.; Ming, L.-J. *J. Biol. Inorg. Chem.* **2002**, *7*, 600–610.
(42) Park, H. I.; Ming, L.-J. *J. Inorg. Biochem.* **1998**, *72*, 57–62.

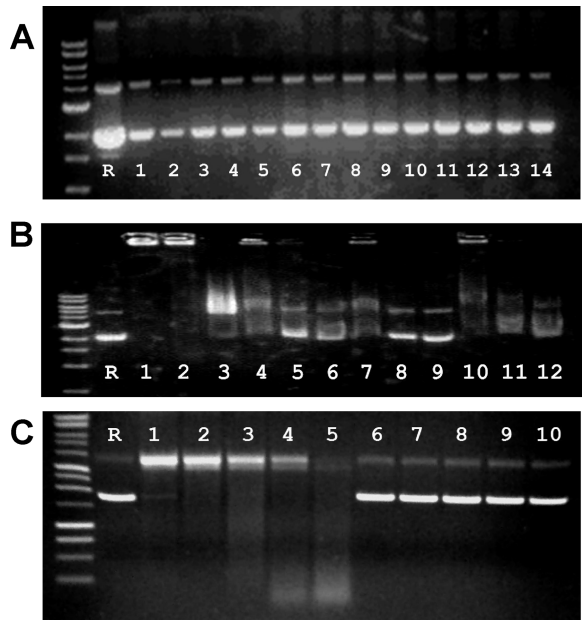

Figure 10. (A) Apo-Bc + plasmid (pQE30Xa of ~3.5 kb, Qiagen). Each lane contains 150 ng plasmid + varying concentration of apo-Bc ranging from 1 to 33 mM (R, reference plasmid; 1, 33 mM; 2, 25 mM; 3−14, decrease by 2 mM each toward the right from 23 to 1 mM). (B) Metallobacitracin + plasmid. Cu(II)−Bc (Lanes 1−3); Mn(II)−Bc (lanes 4−6); Ni(II)−Bc (Lanes 7−9); Co(II)−Bc (Lanes 10−12). The concentrations of metallobacitracins are 9, 3, and 1 mM from the left lane. (C) 170 ng plasmid + 75 μM Cu(II)−Bc in the presence of 5.0 mM ascorbic acid (lanes 1−5) and control (lanes 6−10; plasmid + 75 μM Cu(II) + 5.0 mM ascorbic acid) with incubation times of 5, 10, 20, 40, and 60 min from left to right. Conditions: 100.0 mM HEPES at pH 7 and 37 °C.

and swings to the opposite direction to form a H-bond with NH of Ile-5 or H-bonded to the bound pyrophosphate, and (c) the hydrophobic pocket wherein Ile-5-Phe-9 separation (based on Cδ−C4) increases from 3.91 to 7.55 Å to compensate for the hydrophobic farnesyl chain.

DNA Binding and Cleavage. Since Co(II)−Bc can bind phospho-moieties, potential DNA binding and cleavage by metallobacitracins was investigated. Bc was reported to interact with DNA and polynucleotides and affect cleavage of phage DNA by the restriction enzymes *Hin*dIII and *Sma*I; however, the role of metal ions in such interaction was not investigated.[43] Incubation of plasmid DNA with various amounts of apo-Bc did not reveal noticeable changes, reflecting lack of interaction (Figure 10A). Conversely, the presence of various metal complexes of Bc results in retardation in DNA migration, clearly shown at higher concentrations of metallobacitracins (e.g., lanes 1, 4, 7, and 10, Figure 10B), which indicates metal ions play an important role for bacitracin interaction with DNA.

In the presence of 5.0 mM ascorbic acid, plasmid DNA is rapidly cleaved by 75.0 μM Cu(II)−Bc (Figure 10C). The supercoiled form is nearly completely nicked in 5 min (line 1), the formation of the linear form is visible at 10 min (lane 2), and the plasmid is completely cleaved in 60 min (lane 5). The results indicate a predominant single-stranded DNA cleavage since the linear form becomes visible only in the later stage of the cleavage. There is not much change of the plasmid in the same time period (lanes 6−10) in the control, reflecting a higher efficacy of Cu(II)−Bc than Cu(II) in oxidative DNA damage.

(43) Permogorov, V. I.; Rebentish, B. A.; Lukin, A. A.; Tiaglov, B. V. *Mol. Biol. (Moscow)* **1985**, *19*, 936–940.

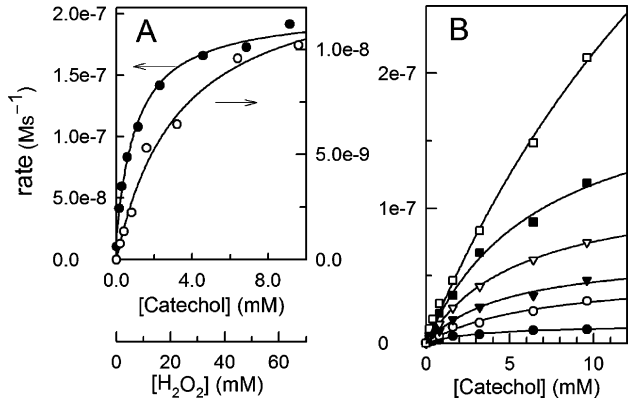

Figure 11. (A) oxidation of catechol of various concentrations by 2.0 μM Cu(II)−Bc (○, right scale) and 0.7 mM catechol by 20 μM Cu(II)−Bc with various amount of hydrogen peroxide (●, left scale). (B) H_2O_2 influence on catechol oxidation by 2.0 μM Cu(II)−Bc; [H_2O_2] = 0, 2, 4, 8, 16, and 32 mM from bottom. Conditions: 100 mM HEPES buffer at pH 7.0 and 25.0 °C.

In the presence of ascorbic acid, Cu(II)−Bc is reduced to Cu(I)−Bc which can bind O_2 to form superoxo−Cu(II)−Bc complex which may do damage to DNA. Alternatively, O_2 binding may eventually yield H_2O_2 and generates •OH radical that harms DNA, analogous to the well-established Cu(II)−1,10-phenanthroline chemistry under reduction conditions.[44] Damage of DNA by Bc in the presence of an iron or copper salt was previously observed via the detection of thiobarbituric acid-reactive material and observation of oxidative modification to bases.[45,46] Since the formation constant for Cu(II)−Bc is higher than that for Zn(II)−Bc determined by electrophoresis and microcalorimetry,[22,23] Bc can be expected to favorably form a Cu(II) complex and exhibit oxidation chemistry.

Oxidative Activity. The oxidation chemistry of Cu(II)−Bc was further investigated by the use of the prototypical substrate catechol (CA). The formation of the oxidized *o*-quinone product is followed by monitoring the red adduct formed between the product and the *o*-quinone-specific indicator MBTH. The catechol oxidation by the Cu(II)−Bc complex in the air increases with [CA] and eventually reaches a plateau (○, Figure 11A), suggesting an enzyme-like pre-equilibrium kinetics (eq 1). However, since catechol oxidation is a two-electron transfer process, an extra oxidative agent should be involved which can be dioxygen in the air and/or another Cu(II)−Bc molecule. The mechanism is further discussed later. The rate law for this reaction can be described according to eq 2, assuming [(Cu^{II}−Bc)−CA] ≪ [CA] ~ [CA]$_o$,

$$\text{Cu}-\text{Bc} + \text{CA} \underset{k_{-1}}{\overset{k_1}{\rightleftharpoons}} [((\text{Cu}-\text{Bc}) + \text{CA})] \xrightarrow{[\text{O}]} \xrightarrow{[k_{cat}]} \text{Cu}-\text{Bc} + o\text{-quinone} \quad (1)$$

$$v_0 = v_{bk} + \frac{V_{max}[\text{CA}]}{K_{CA} + [\text{CA}]} \quad (2)$$

where v_0 and V_{max} are the measured and maximum rate, respectively, k_{cat} (= V_{max}/[Cu(II)−Bc]) is the observed first-order rate constant (the turnover number), and K_{CA} = (k_{cat} +

(44) Sigman, D. S. *Acc. Chem. Res.* **1986**, *19*, 180–186.
(45) Quinlan, G. J.; Gutteridge, J. M. C. *Free Rad. Res.* **1989**, *7*, 37–44.
(46) Quinlan, G. J.; Gutteridge, J. M. C. *Biochem. Pharmacol.* **1991**, *27*, 1595–1599.

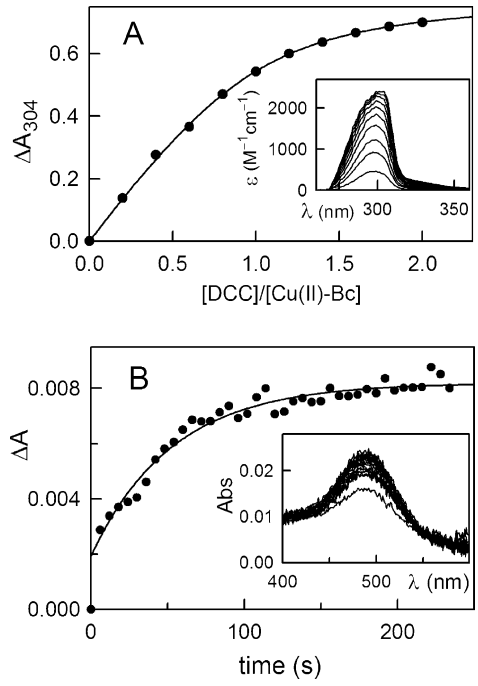

Figure 12. (A) DCC binding to Cu^{II}−Bc in DMF to afford the Cu(II)−Bc−DCC complex with an absorption at 304 nm (with 0.2 equiv increment; inset). Plot of the change in absorbance with respect to the amount of DCC yield an affinity constant of 2.40×10^4 M^{-1}. (B) Oxidation of 2.5 mM catechol by 0.10 mM Cu(II)−Bc under anaerobic conditions. The reaction was determined immediately after the addition of Cu(II)−Bc via the change in absorbance at 500 nm (inset) with time, which was fitted to the first-order rate law to yield $k_o = 0.021 \pm 0.004$ s^{-1}.

$k_{-1})/(k_1)$ is the virtual dissociation constant of the ternary (Cu−Bc)−CA complex. The data fit well to eq 2 to afford $k_{cat}(CA) = 7.0 \times 10^{-3}$ s^{-1}, $K_{CA} = 3.3$ mM, and a second-order rate constant $k_{cat}/K_{CA} = 2.1$ M^{-1} s^{-1} for the reaction taking place in air-saturated solution at 25 °C (Figure 11A). There is significant 1.5×10^4-fold increase in CA oxidation rate in terms of the first-order rate constant relative to the auto-oxidation rate constant of catechol (4.74×10^{-7} s^{-1}).[47]

The interaction between the catechol substrate and Cu(II)−Bc is confirmed by the slow substrate 4,5-dichlorocatechol (DCC), which results in a charge-transfer band at 304 nm (inset, Figure 12A) upon binding to Cu(II)−Bc. The change in absorbance at 304 nm versus [DCC] can be fitted to a 1:1 binding pattern of Cu(II)−Bc + DCC ⇌ [Cu(II)−Bc]−DCC to afford an affinity constant of 2.40×10^4 M^{-1} (Figure 12A). Under the equilibrium of $xM + yL \rightleftharpoons [M_x-L_y]$, the stoichiometry of x:y in the complex can be determined with the Job plot.[32,33] A plot of the absorption of the DCC−(Cu−Bc) complex at 310 nm versus the mole fraction of DCC (X_{DCC}) shows a maximum around 0.5 (○, Figure 13), which can be fitted to the stoichiometry of (Cu−Bc):DCC = 1:1 (i.e., X_{Cu-Bc}:$X_{DCC} = 0.5$:0.5). The 1:1 stoichiometry reflects that a mononuclear catalysis is taking place wherein each substrate is bound to and oxidized by one Cu(II)−Bc complex.

The presence of equilibrium between CA and Cu−Bc to form the reactive intermediate complex CA−(Cu−Bc) during the pre-equilibrium stage of CA oxidation (eq 1) allows further investigation of the reaction mechanism of the reaction by the Job plot, herein dubbed "mechanistic Job plot". Since this

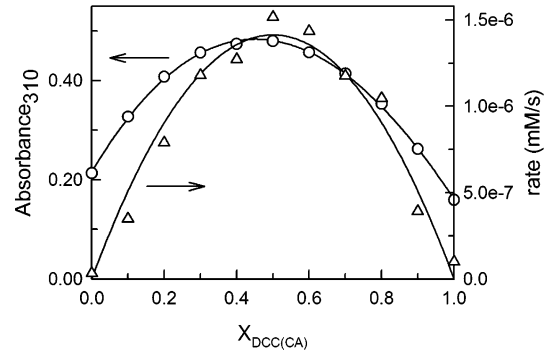

Figure 13. (○; Left scale) Optical Job plot of DCC binding to Cu(II)−Bc, which is fitted to the stoichiometry of Cu(II)−Bc:DCC = 1:1. (Δ; Right scale) "Mechanistic Job plot" with the activity of CA oxidation as the output, which is fitted to the stoichiometry of Cu(II)−Bc:CA = 1:1. The total concentration of [Cu−Bc] + [DCC] is 0.50 mM (○) and [Cu−Bc] + [CA] is 50 μM (Δ) in 100.0 mM HEPES buffer at pH 7.0 and 25.0 °C. $X_{DCC(CA)}$ is the mole fraction of DCC (○) or CA (Δ).

complex is the active form during the reaction, the mechanistic Job plot is accomplished by monitoring the activity of CA oxidation. In Cu-mediated oxidative catalysis, the reaction may follow a mononuclear or a dinuclear mechanism which is reflected by the stoichiometry of the intermediate complex CA_x−$(Cu-Bc)_y$ determined by the mechanistic Job plot, in which a stoichiometry of x:y = 1:1 or 1:2 reflects a mononuclear or a dinuclear catalysis. The data from the plot show a maximum at around $X_{CA} = 0.5$ which can be fitted to 1:1 stoichiometry (Δ, Figure 13). Thus, the active species has a stoichiometry of CA:(Cu−Bc) = 1:1 (i.e., X_{CA}:$X_{Cu-Bc} = 0.5$:0.5), consistent with a mononuclear mechanism for the oxidation of CA by Cu(II)−Bc which corroborates with the conclusion drawn from DCC binding.

Dioxygen binding and oxidation chemistry of synthetic mononuclear Cu(II) complexes have been studied with several spectroscopic techniques and theoretical calculations.[48] Since the oxidation of catechol to *o*-quinone is a 2-electron transfer process, the involvement of dioxygen in recycling of the metal center between Cu(I) and Cu(II) is expected. Thus, the oxidative activity of Cu(II)−Bc was determined in the absence of dioxygen, wherein the reaction of 2.5 mM CA quickly reaches a plateau (Figure 12B) to yield *o*-quinone product (trapped by MBTH) with an observed rate constant $k_o = 0.021 \pm 0.004$ s^{-1}. This rate constant is significantly larger than the k_{cat} value from the aerobic experiment above, which indicates a faster reaction has already occurred prior to the aerobic reaction when dioxygen is involved, probably due to direct oxidation of CA by the Cu(II) center. In this case, Cu(II) is reduced and can bind dioxygen in the solution to continue the catalytic cycle. However, this anaerobic reaction is quite inefficient which produces only about 0.77 μM of the product at the equilibrium state (when it reaches the plateau), corresponding to a very small equilibrium constant $K_{eq} = 3.2 \times 10^{-6}$ based on the concentrations at the plateau under the experimental conditions.

There are two modes for dioxygen binding to a metal center, end-on (η^1) and side-on (η^2) binding.[48−51] The steric effect is

(47) da Silva, G. F. Z.; Ming, L.-J. *Angew. Chem., Int. Ed.* **2005**, *44*, 5501–5504.
(48) Itoh, S. *Curr. Opin. Chem. Biol.* **2006**, *10*, 115–122.
(49) Spencer, D. J. E.; Aboelella, N. W.; Reynolds, A. M.; Holland, P. L.; Tolman, W. B. *J. Am. Chem. Soc.* **2002**, *124*, 2108–2109.
(50) Aboelella, N. W.; Kryatov, S. V.; Gherman, B. F.; Brennessel, W. W.; Young, V. G., Jr.; Sarangi, R.; Rybak-Akimova, E. V.; Hodgson, K. O.; Hedman, B.; Solomon, E. I. *J. Am. Chem. Soc.* **2004**, *126*, 16896–16911.

an important factor in controlling dioxygen binding to a metal center, such as the mononuclear Cu(II)−superoxo complex with a side-on binding mode induced by steric effect of the ligand which prevents the formation of a dinuclear center.[52] The crystal structure of peptidylglycine α-hydroxylating monooxygenase shows end-on O_2 binding to one of its mononuclear Cu centers.[53] In the presence of a bound bidentate catechol, dioxygen may only bind to the Cu(II)−Bc center (containing three endogenous ligands) via an end-on mode as Cu(II)−O_2^- or Cu(II)−OOH due to coordination crowding. Alternatively, a ligand-centered pathway as found in Fe-containing catechol dioxygenase[54] is likely to take place, wherein a semiquinone formed after one-electron transfer as a metal-bound form or as a free form in solution is attacked directly by O_2. Conclusion of the mechanism awaits more detailed investigation in the future.

Hydrogen peroxide can bind to a Cu(II) center to afford a Cu(II)−peroxo center, which is able to oxidize a bound substrate. The oxidation rate of CA was observed to increase with the amount of H_2O_2 and reaches a plateau at higher concentrations of H_2O_2 (●, Figure 11A). The saturation profile indicates a pre-equilibrium kinetics, reflecting direct H_2O_2 binding to the metal center to form the intermediate ternary complex H_2O_2−[(Cu−Bc)−CA] for the oxidation of CA. The data can be fitted to eq 2 with [S] = [H_2O_2] to afford $k_{cat}(H_2O_2)$ = 9.4 × 10^{-3} s^{-1} and an apparent dissociation constant $K_{H_2O_2}$ of 7.5 mM for the dissociation of H_2O_2 from the ternary complex H_2O_2−[(Cu−Bc)−CA] at [CA] = 0.7 mM.

The oxidation rate of catechol by Cu(II)−Bc increases with [H_2O_2] (Figure 11B). The presence of 32.0 mM H_2O_2 in the assay increased k_{cat}(CA) and k_{cat}(CA)/K_{CA} values (0.38 s^{-1} and 14.7 M^{-1} s^{-1}) by 55 and 7 times, respectively. Hence, the significant increase in K_{CA} in the presence of H_2O_2 is attributed to the dramatic increase in k_{cat} value. Since both CA and H_2O_2 can independently bind to the Cu(II) center (Figure 11A), it is essential to determine how the binding of one affects that of the other which can be analyzed by the Hanes plot, from which the apparent binding constants for both substrates and the intrinsic binding constant for one substrate can be calculated according to eq 3:[55,56]

$$\frac{[CA]}{v_0} = \frac{\left(1 + \frac{K^{App}_{H_2O_2}}{[H_2O_2]}\right)}{V_{max}}[CA] + \frac{K^{App}_{CA}}{V_{max}}\left(1 + \frac{K^{Int}_{H_2O_2}}{[H_2O_2]}\right) \quad (3)$$

where $K^{Int}_{H_2O_2}$ is the intrinsic binding constant for H_2O_2, $K^{App}_{H_2O_2}$ and K^{App}_{CA} are the apparent binding constants for H_2O_2 and catechol, respectively, and v_0 and V_{max} are the experimental and maximum velocity, respectively (Figure 14A). The ratio between the corresponding apparent and intrinsic equilibrium constants for each substrate can suggest how the binding of one substrate affects the binding of another. Then, the secondary plots of the fitted slope $(1/V_{max})(1 + (K^{App}_{H_2O_2}/[H_2O_2]))$ (Figure 14B) and

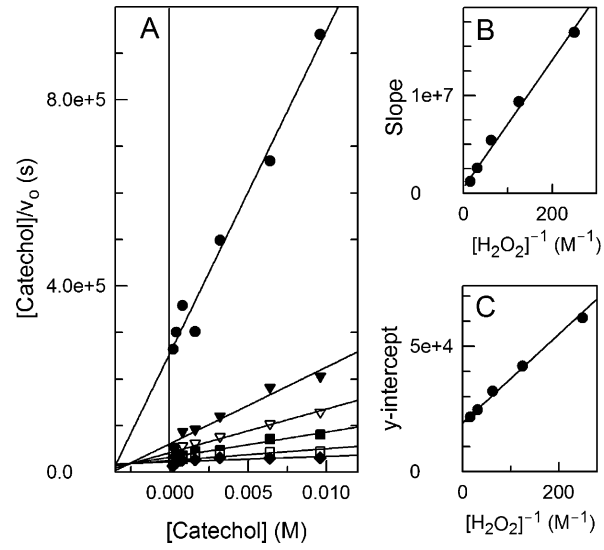

Figure 14. (A) Hanes analysis of the oxidation of catechol by Cu(II)−Bc at different concentrations of H_2O_2 (kinetic data from Figure 11B). [H_2O_2] = 0, 4, 8, 16, 32, and 64 mM from the bottom. Plots (B) and (C) are the secondary plots of the slope and *y*-intercept values, respectively, obtained from plot (A) with respect to $[H_2O_2]^{-1}$.

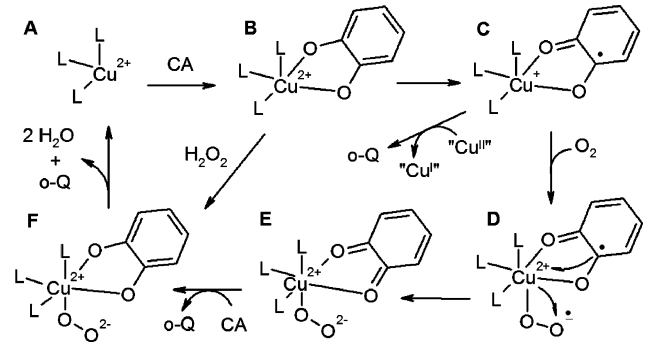

Figure 15. Proposed mechanism for catechol oxidation by Cu(II)−Bc through a mononuclear Cu(II) center in the presence of O_2 (steps **A** through **F**) or in the presence of H_2O_2 (steps **A**, **B**, and **F**).

y-intercept $(K^{App}_{CA}/V_{max})(1 + (K^{Int}_{H_2O_2}/[H_2O_2]))$ (Figure 14C) versus $1/[H_2O_2]$ afford the two apparent equilibrium constants $K^{App}_{H_2O_2}$ = 52.8 mM and K^{App}_{CA} = 17.8 mM for the dissociation of H_2O_2 and CA, respectively, from the ternary complex H_2O_2−[CA−(Cu−Bc)] and the intrinsic equilibrium constant $K^{Int}_{H_2O_2}$ = 7.8 mM for the dissociation of H_2O_2 from the complex H_2O_2−(Cu−Bc). The ratio between the apparent and intrinsic binding constants is 5.37 for catechol (K^{App}_{CA}/K_{CA}) and 6.74 for H_2O_2 ($K^{App}_{H_2O_2}/K^{Int}_{H_2O_2}$), which suggests that the affinity of CA or H_2O_2 to Cu−Bc is significantly decreased by each other. The reduction in the effectiveness of binding may be due to inability of the Cu(II) center to further expand its coordination sphere. Thus, the observation described herein is more consistent with an end-on binding mode of O_2^- due to the steric effect casued by a plausible bidentate catechol binding to the metal center.

A mechanism is proposed for the oxidation of catechol by Cu(II)−Bc through a mononuclear Cu center (Figure 15). First, catechol binds to the Cu(II) center in a bidentate manner (**A**, **B**), followed by electron redistribution to Cu(II) to afford a transient Cu(I)−semiquinone complex (**C**). The complex (**C**) binds O_2 and followed by electron transfer to O_2, yielding a superoxo−Cu(II)−semiquinone intermediate (**D**). The bound semiquinone is further oxidized to yield *o*-quinone and a

(51) Maiti, D.; Fry, H. C.; Woertink, J. S.; Vance, M. A.; Solomon, E. I.; Karlin, K. D. *J. Am. Chem. Soc.* **2007**, *129*, 264–265.
(52) Fujisawa, K.; Tanaka, M.; Moro-oka, Y.; Kitajima, N. *J. Am. Chem. Soc.* **1994**, *116*, 12079–12080.
(53) Prigge, S. T.; Eipper, B. A.; Mains, R. E.; Amzel, L. M. *Science* **2004**, *304*, 864–867.
(54) Que, L.; Ho, R. Y. N. *Chem. Rev.* **1996**, *96*, 2607–2624.
(55) Segel, I. H. *Enzyme Kinetics: Behavior and Analysis of Rapid Equilibrium and Steady-State Enzyme Systems*; John Wiley & Sons, Inc.: New York, U.S.A, 1993.
(56) Leskovac, V. *Comprehensive Enzyme Kinetics*; Kluwer/Plenum: Boston, U.S.A., 2002.

Cu(II)−peroxo center (**E**), which bind another CA and goes through another catalytic cycle (**F**) since a peroxo can take 2 electrons from the substrate to yield $2H_2O$ and quinone. In the presence of H_2O_2, it binds directly to the [(Cu−Bc)−CA] complex (**B**, **F**) to afford the ternary complex peroxo−[(Cu−Bc)−CA] (**F**), followed by CA oxidation to complete the catalytic cycle.

Concluding Remarks

Although Co(II)−Bc is kinetically labile, like many simple Co(II) complexes, as demonstrated by the detection of exchange-pairs in the 1D and 2D NMR saturation transfer experiments,[24] its several pyrophosphate-containing ternary complexes are kinetically inert. This inertness may render the metallobacitracin-bound lipid pyrophosphates kinetically unavailable for the glycosylation process, thus effectively inhibits bacterial cell wall synthesis. The results corroborate the proposed antibiotic mechanism.[25] The observation of binding of pyrophsophate and derivatives to Co(II)−Bc also implies that metallobacitracin may possibly bind several ubiquitous pyrophosphate-containing nucleotides, such as ADP, NAD^+, FAD, and coenzyme A, to form complexes that can disturb energetic and metabolic regulations and influence a broader spectrum of homeostasis in the cells. In addition to its antibiotic activities, Bc also exhibits toxic effect toward nauplii and cysts of brine shrimp[57] and affects erythroid differentiation.[58] The oxidative activities and interactions with different biomolecules may be significant for the observed bioactivities of this metallopeptide. Future studies will further clarify this hypothesis and corroborate the important role of metal ions in the action of this metallopeptide.

Acknowledgment. Our studies of metallopeptides were supported by the National Science Foundation (CHE-0718625).

JA910504T

(57) Migliore, L.; Civitareale, C.; Brambilla, G.; DiDelupis, G. D. *Water Res.* **1997**, *31*, 1801–1806.
(58) Foresti, M.; Migliore, L. *Cell Biol. Toxicol.* **1993**, *9*, 377–384.